*inorganics*

MDPI

*Article*

# Hidden Magnetic-Field-Induced Multiferroic States in A-Site-Ordered Quadruple Perovskites $RMn_3Ni_2Mn_2O_{12}$: Dielectric Studies

**Alexei A. Belik [1,*], Ran Liu [1,2,3] and Kazunari Yamaura [1,2]**

[1] Research Center for Materials Nanoarchitectonics (MANA), National Institute for Materials Science (NIMS), Namiki 1-1, Tsukuba 305-0044, Ibaraki, Japan; liu.ran@sanken.osaka-u.ac.jp (R.L.); yamaura.kazunari@nims.go.jp (K.Y.)
[2] Graduate School of Chemical Sciences and Engineering, Hokkaido University, North 10 West 8, Kita-ku, Sapporo 060-0810, Hokkaido, Japan
[3] Institute of Scientific and Industrial Research, Osaka University, Mihogaoka 8-1, Ibaraki 567-0047, Osaka, Japan
* Correspondence: alexei.belik@nims.go.jp

## Abstract

The appearance of spin-induced ferroelectric polarization in the so-called type-II multiferroic materials has received a lot of attention. The nature and mechanisms of such polarization were intensively studied using perovskite rare-earth manganites, $RMnO_3$, as model systems. Later, multiferroic properties were discovered in some $RFeO_3$ perovskites and possibly in some $RCrO_3$ perovskites. However, $R_2NiMnO_6$ double perovskites have ferromagnetic structures that do not break the inversion symmetry. It was found recently that more complex magnetic structures are realized in A-site-ordered quadruple perovskites, $RMn_3Ni_2Mn_2O_{12}$. Therefore, they have the potential to be multiferroics. In this work, dielectric properties in magnetic fields up to 9 T were investigated for such perovskites as $RMn_3Ni_2Mn_2O_{12}$ with R = Ce to Ho and for $BiMn_3Ni_2Mn_2O_{12}$. The samples with R = Bi, Ce, and Nd showed no dielectric anomalies at all magnetic fields, and the dielectric constant decreases with decreasing temperature. The samples with R = Sm to Ho showed qualitatively different behavior when the dielectric constant started increasing with decreasing temperature below certain temperatures close to the magnetic ordering temperatures, $T_N$. This difference could suggest different magnetic ground states. The samples with R = Eu, Dy, and Ho still showed no anomalies on the dielectric constant. On the other hand, peaks emerged at $T_N$ on the dielectric constant in the R = Sm sample from about 2 T up to the maximum available field of 9 T. The Gd sample showed peaks on dielectric constant at $T_N$ between about 1 T and 7 T. Transition temperatures increase with increasing magnetic fields for R = Sm and decrease for R = Gd. These findings suggest the presence of magnetic-field-induced multiferroic states in the R = Sm and Gd samples with intermediate ionic radii. Dielectric properties at different magnetic fields are also reported for $Lu_2NiMnO_6$ for comparison.

**Keywords:** A-site-ordered quadruple perovskites; B-site double ordering; multiferroics; dielectric constant



Academic Editor: Chiara Dionigi

Received: 3 September 2025
Revised: 16 September 2025
Accepted: 22 September 2025
Published: 25 September 2025

**Citation:** Belik, A.A.; Liu, R.; Yamaura, K. Hidden Magnetic-Field-Induced Multiferroic States in A-Site-Ordered Quadruple Perovskites $RMn_3Ni_2Mn_2O_{12}$: Dielectric Studies. *Inorganics* **2025**, *13*, 315. https://doi.org/10.3390/inorganics13100315



## 1. Introduction

The appearance of spin-induced ferroelectric polarization in the so-called type-II multiferroic materials has received a lot of attention in the literature [1–7]. Because ferroelectric

polarization appears as a result of a magnetic ordering, there is a strong magnetoelectric coupling in such materials, allowing for the control of ferroelectric polarization via a magnetic field and vice versa [8,9]. The nature and mechanisms of such polarization were intensively studied using perovskite-structure rare-earth (R) manganites, $RMnO_3$, as model systems [10–13]. Only some members of the $RMnO_3$ family with specific magnetic structures develop spin-induced ferroelectric polarization, for example, in $RMnO_3$ (R = Tb to Dy) with modulated sinusoidal/spiral antiferromagnetic (AFM) ordering and in $RMnO_3$ (R = Ho to Lu) with the so-called E-type magnetic ordering. Multiferroic properties were discovered in some $RFeO_3$ perovskites [14–20] and possibly in some $RCrO_3$ perovskites [21–23]. While the multiferroic properties of $RFeO_3$ at very low temperatures, where they are caused by additional magnetic orderings of the $R^{3+}$ sublattice, are well established [14–16], the existence of ferroelectric polarization at higher temperatures in $RFeO_3$ and $RCrO_3$ is still under debate [18,19,24].

All $R_2NiMnO_6$ double perovskites [25–41] have simple ferromagnetic (FM) structures (in the first approximation), which do not break inversion centers and do not produce spin-induced ferroelectric polarization. Nevertheless, there are a few reports with claims of spin-induced ferroelectric properties in $R_2NiMnO_6$ double perovskites [25,26]. However, such claims were not confirmed [27], and therefore, they are still controversial. The use of cations smaller than $Lu^{3+}$ ($r_{XIII}(Lu^{3+})$ = 0.977 Å [42]) at the R sites (such as $Sc^{3+}$ with $r_{XIII}(Sc^{3+})$ = 0.870 Å and $In^{3+}$ with $r_{XIII}(In^{3+})$ = 0.92 Å [42]) further reduces Ni–O–Mn bond angles in the $R_2NiMnO_6$ series, weakens the strength of direct FM Ni–Mn exchange interactions, and stabilizes complex AFM structures. For example, $Sc_2NiMnO_6$ demonstrates two AFM transitions [43]. The dielectric constant of $Sc_2NiMnO_6$ starts increasing with decreasing temperature when approaching $T_{N1}$ = 35 K and shows a sharp drop below $T_{N2}$ = 17 K. On the other hand, pyroelectric current measurements did not show the development of spin-induced ferroelectric polarization [43]. One AFM transition with an incommensurate structure was found in $In_2NiMnO_6$ at $T_N$ = 26 K [44,45], and this compound shows spin-induced ferroelectric polarization [45]. Ferroelectric polarization is suppressed by magnetic fields above 6 T. The dielectric constant of $In_2NiMnO_6$ basically decreases with decreasing temperature between 5 K and 300 K, and a sharp peak is only observed at $T_N$ [45]. It turned out that $Lu_2NiMnO_6$ is located near a phase boundary between FM and AFM states on the phase diagram of the $R_2NiMnO_6$ double perovskites, and a moderate pressure can induce a transition from an FM state to an incommensurate AFM state [35].

The $R_2NiMnO_6$ family of B-site-ordered double perovskites was recently extended further to a subfamily of A-site-ordered quadruple perovskites [46–51] with the composition of $RMn_3Ni_2Mn_2O_{12}$ with R = Bi [52], La [53,54], Ce [52], Nd [55], Sm [55], Gd [55], Dy [55], and Ho [52]. $RMn_3Ni_2Mn_2O_{12}$ behaves differently from $R_2NiMnO_6$. For example, $LaMn_3Ni_2Mn_2O_{12}$ has two magnetic transitions at $T_N$ = 46 K and $T_C$ = 34 K [53] (similar to $Sc_2NiMnO_6$ and in comparison with other members of the $R_2NiMnO_6$ family (R = La to Lu)). Complex magnetic structures are realized in $LaMn_3Ni_2Mn_2O_{12}$ [53]. $NdMn_3Ni_2Mn_2O_{12}$ already shows one magnetic transition at $T_N$ = 26 K [55]. Net FM components are developed at the ground states of $RMn_3Ni_2Mn_2O_{12}$ with R = La and Nd. On the other hand, AFM ground states are basically realized in $RMn_3Ni_2Mn_2O_{12}$ with R = Sm to Ho. Complex AFM ground states are promising for the realization of spin-induced ferroelectric polarization. However, detailed dielectric studies of the $RMn_3Ni_2Mn_2O_{12}$ perovskites have not been performed yet.

Therefore, in this work, we investigated nearly all members of the $RMn_3Ni_2Mn_2O_{12}$ family by performing detailed measurements of dielectric constant in different magnetic fields up to 9 T. While no dielectric constant anomalies were found at a zero magnetic field in all samples, peaks emerge in the dielectric constant in the R = Sm and Gd samples

in intermediate ranges of the magnetic field. These observations suggest the presence of magnetic-field-induced multiferroic states in the R = Sm and Gd samples. Basic physical properties of $EuMn_3Ni_2Mn_2O_{12}$ and dielectric properties at different magnetic fields for $Lu_2NiMnO_6$ are also reported for comparison.

## 2. Results and Discussion

### *2.1. R = Bi, Ce, and Nd*

Temperature dependence of dielectric constant and loss tangent of $BiMn_3Ni_2Mn_2O_{12}$ in different magnetic fields is shown in Figure 1. Very weak effects of magnetic fields on dielectric constant values were observed in agreement with the reported weak effects of magnetic fields on specific heat values [52]. No dielectric constant anomalies were observed at $T_N$ = 36 K [52] of $BiMn_3Ni_2Mn_2O_{12}$.

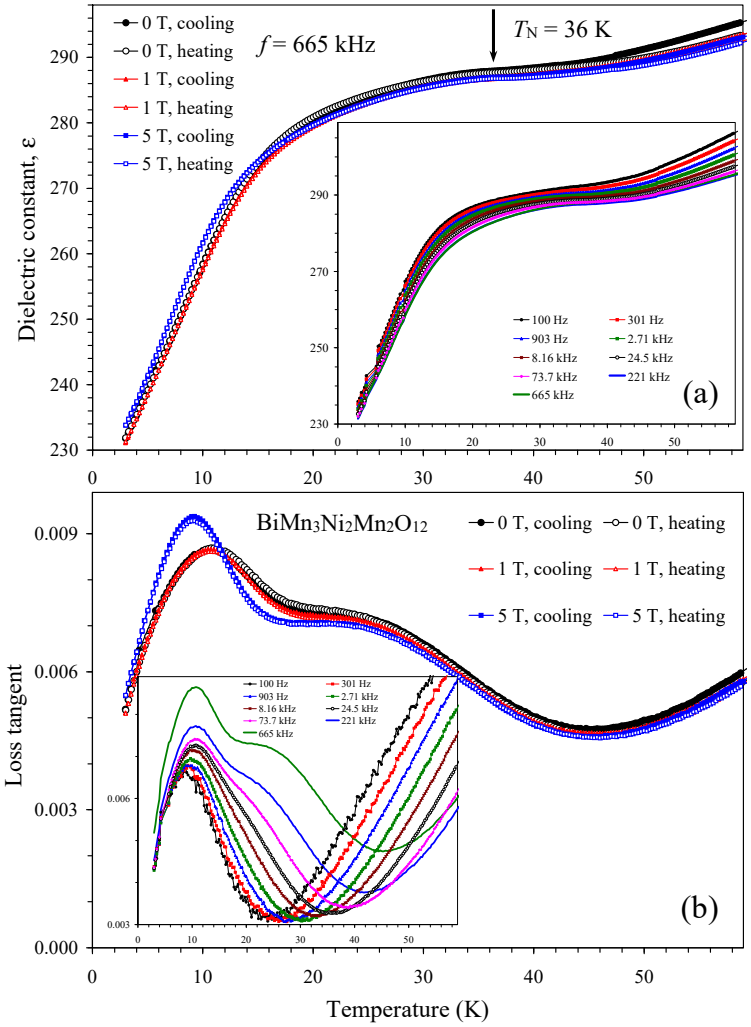


**Figure 1.** (**a**) Temperature dependence of dielectric constant of $BiMn_3Ni_2Mn_2O_{12}$ at one frequency of 665 kHz and different magnetic fields of 0, 1, and 5 T on cooling and heating. The inset shows the temperature dependence of the dielectric constant at different frequencies at $H$ = 0 T (on cooling). The arrow shows a magnetic transition temperature [52]. (**b**) Temperature dependence of loss tangent of $BiMn_3Ni_2Mn_2O_{12}$ at one frequency of 665 kHz and different magnetic fields of 0, 1, and 5 T on cooling and heating. The inset shows the temperature dependence of the loss tangent at different frequencies at $H$ = 0 T (on cooling).

The temperature dependence of the dielectric constant and loss tangent of $CeMn_3Ni_2Mn_2O_{12}$ (Figure 2) and $NdMn_3Ni_2Mn_2O_{12}$ (Figures 3 and S1) were qualita-

tively similar. The dielectric constant slightly decreased with decreasing temperature, and weak effects of magnetic fields on dielectric constant values were observed below about 60 K. Loss tangent of both samples showed broad anomalies below about 15 K (at the frequency of 665 kHz). No dielectric constant anomalies were observed at their magnetic transition temperatures of 27 K and 33 K (for R = Ce [52]) and 26 K (for R = Nd [55]). In dielectric insulator materials without any ferroelectric or ferroelectric-like transitions, the dielectric constant is usually temperature independent or slightly decreases with decreasing temperature. Therefore, the temperature dependence of the dielectric constant of the R = Ce and Nd samples is typical for ordinary insulators.

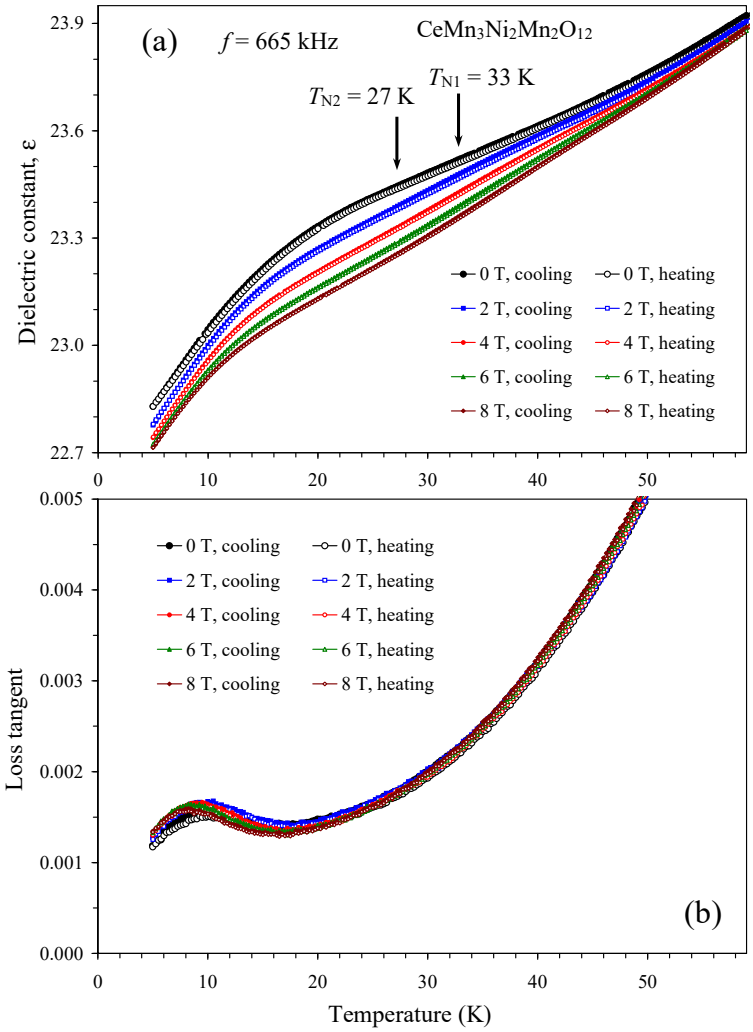


**Figure 2.** (**a**) Temperature dependence of dielectric constant of $CeMn_3Ni_2Mn_2O_{12}$ at one frequency of 665 kHz and different magnetic fields of 0, 2, 4, 6, and 8 T on cooling and heating. Arrows show magnetic transition temperatures [52]. (**b**) Temperature dependence of loss tangent of $CeMn_3Ni_2Mn_2O_{12}$ at one frequency of 665 kHz and different magnetic fields of 0, 2, 4, 6, and 8 T on cooling and heating.

### *2.2. R = Sm*

The temperature dependence of the dielectric constant of $RMn_3Ni_2Mn_2O_{12}$ with R = Sm to Ho was qualitatively different from that of $RMn_3Ni_2Mn_2O_{12}$ with R = Bi, Ce, and Nd because the dielectric constant started increasing with decreasing temperature below about 30–40 K. The increase of the dielectric constant suggests the development of polar correlations. This change in the behavior of the dielectric constant also correlates with the changes in the magnetic properties because net FM components were observed at the ground states of $RMn_3Ni_2Mn_2O_{12}$ with R = Ce and Nd, while AFM ground states are

basically realized in $RMn_3Ni_2Mn_2O_{12}$ with R = Sm to Ho. This change in the behavior of the dielectric constant could reflect different magnetic structures.

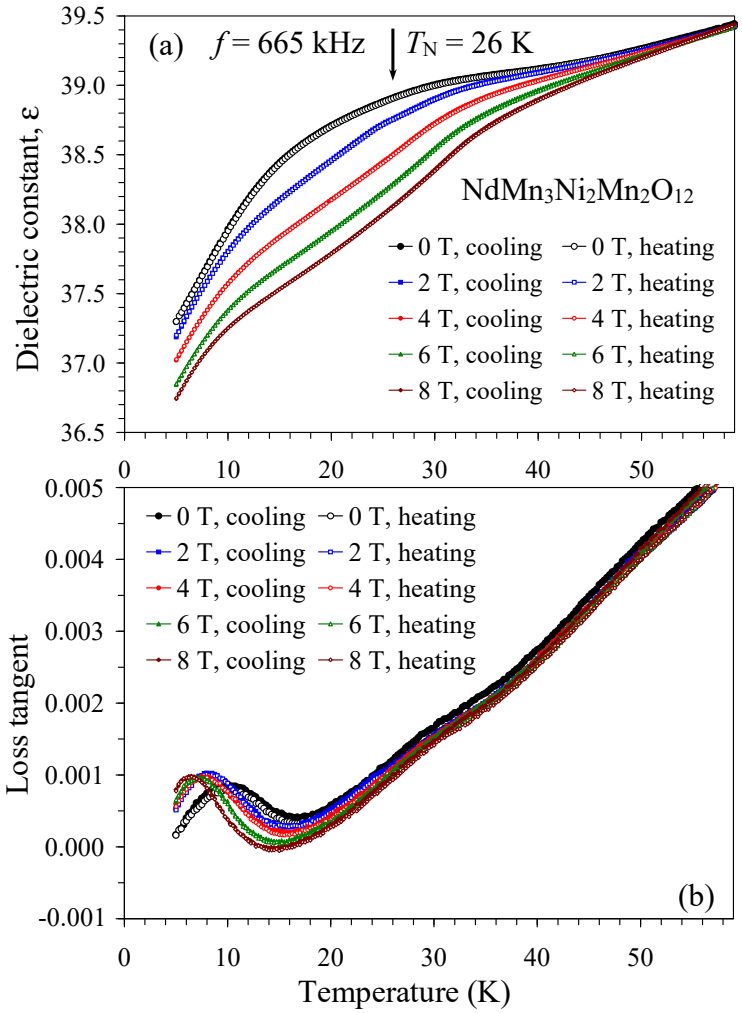


**Figure 3.** (**a**) Temperature dependence of dielectric constant of $NdMn_3Ni_2Mn_2O_{12}$ at one frequency of 665 kHz and different magnetic fields of 0, 2, 4, 6, and 8 T on cooling and heating. The arrow shows a magnetic transition temperature [55]. (**b**) Temperature dependence of loss tangent of $NdMn_3Ni_2Mn_2O_{12}$ at one frequency of 665 kHz and different magnetic fields of 0, 2, 4, 6, and 8 T on cooling and heating.

The dielectric constant and loss tangent of $SmMn_3Ni_2Mn_2O_{12}$ are shown in Figures 4 and S2–S4. At $H$ = 0 T, the dielectric constant and loss tangent of $SmMn_3Ni_2Mn_2O_{12}$ showed no detectable anomalies. However, at $H$ = 2 T, a small kink appears on the dielectric constant, and a peak is visible on the loss tangent near $T_N$ = 23 K. At higher magnetic fields (4–8 T), a small kink on the dielectric constant transforms to a small peak. Peaks on both dielectric constant and loss tangent are moving to higher temperatures with increasing magnetic field in agreement with the similar shift of specific heat anomalies (Figure 5a), confirming their common magnetic origin. Peaks on loss tangent were observed at 20.5 K (at 2 T), 21.5 K (at 4 T), 23.0 K (at 6 T), 24.5 K (at 8 T), and 25.2 K (at 9 T). Almost no hysteresis in the peak positions was observed during cooling and heating. Therefore, the appearance of peaks on both dielectric constant and loss tangent at magnetic fields of 2–9 T suggests the development of spin-induced ferroelectric polarization in $SmMn_3Ni_2Mn_2O_{12}$ at such magnetic fields.

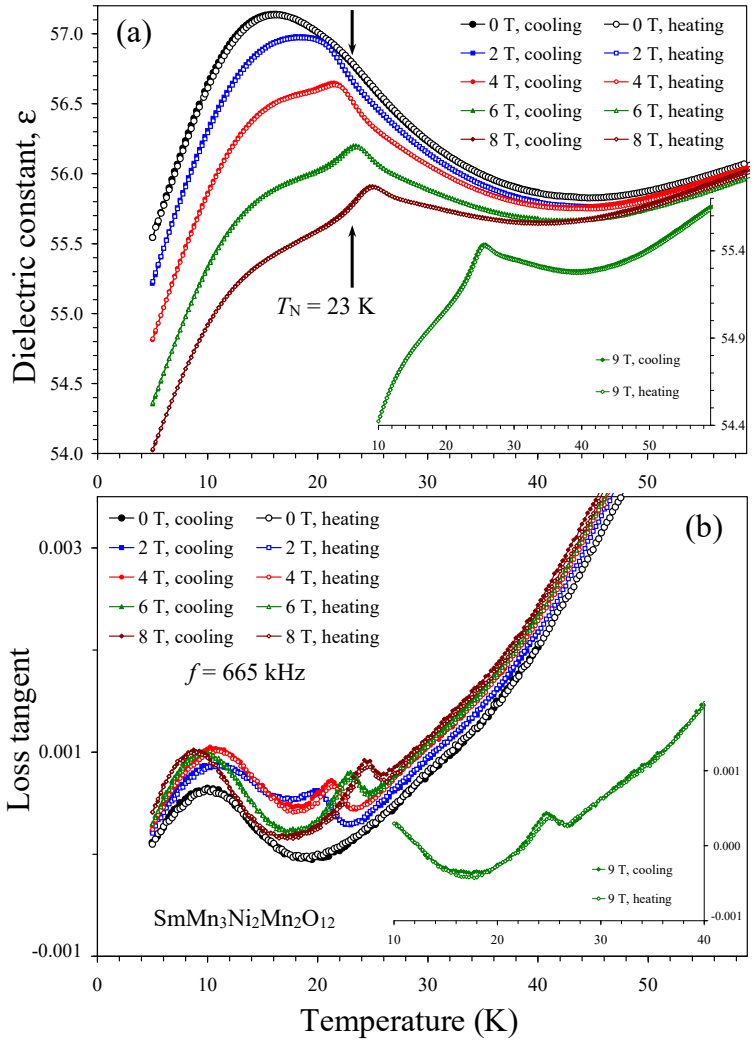


**Figure 4.** (**a**) Temperature dependence of dielectric constant of $SmMn_3Ni_2Mn_2O_{12}$ at one frequency of 665 kHz and different magnetic fields of 0, 2, 4, 6, and 8 T on cooling and heating. The arrow shows a magnetic transition temperature at $H$ = 0 T [55]. (**b**) Temperature dependence of loss tangent of $SmMn_3Ni_2Mn_2O_{12}$ at one frequency of 665 kHz and different magnetic fields of 0, 2, 4, 6, and 8 T on cooling and heating. The insets show data at a magnetic field of 9 T.

### *2.3. R = Eu*

As $EuMn_3Ni_2Mn_2O_{12}$ has not been reported yet, we start with the basic characterization of this compound by other methods. $EuMn_3Ni_2Mn_2O_{12}$ crystallized in a cubic structure of the A-site-ordered quadruple perovskite family [46–51] with $a$ = 7.3430(1) Å. The quality of the standard laboratory X-ray diffraction data (with a measurement speed of 3°/min) did not allow detection of superstructure reflections related to (partial) ordering of $Ni^{2+}$ and $Mn^{4+}$ cations and, therefore, to assign the *Im*-3 or *Pn*-3 space groups. Therefore, we measured X-ray diffraction data with a speed of 0.1°/min between 38° and 44° and could detect a very weak (311) superstructure reflection. This fact suggests that there is a partial ordering of $Ni^{2+}$ and $Mn^{4+}$ cations, and the space group is *Pn*-3, similar to some other members of the $RMn_3Ni_2Mn_2O_{12}$ family [55]. Laboratory X-ray diffraction data also showed the presence of some amounts of $(Eu_{1-x}Mn_x)MnO_3$ impurity (space group *Pnma* with $a$ = 5.5357 Å, $b$ = 7.5834 Å, $c$ = 5.3196 Å; about 6.7 wt. %) and NiO impurity (space group *R*-3*m* with $a$ = 2.9597 Å and $c$ = 7.2374 Å; about 2.5 wt. %). The $(Eu_{1-x}Mn_x)MnO_3$ impurity has a ferrimagnetic transition near 140 K.

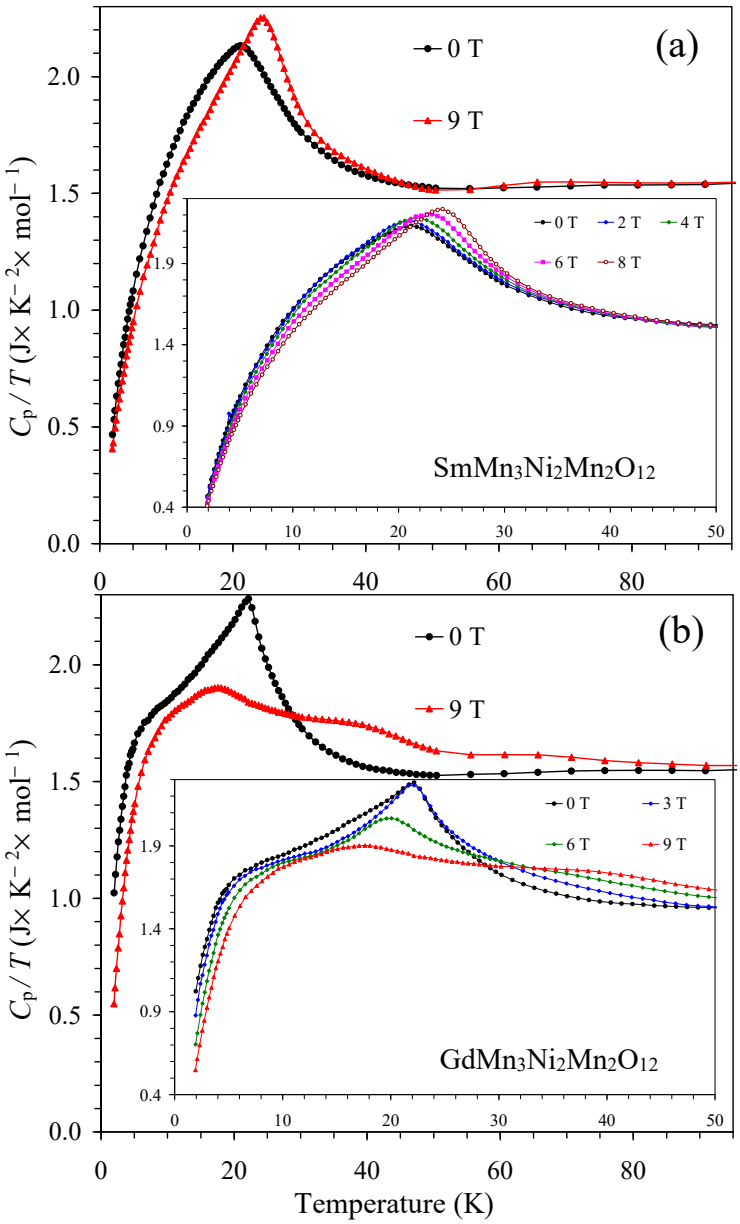


**Figure 5.** (**a**) $C_p/T$ vs. $T$ curves of $SmMn_3Ni_2Mn_2O_{12}$ measured at $H$ = 0 and 9 T on cooling. The inset shows $C_p/T$ vs. $T$ curves at $H$ = 0, 2, 4, 6, and 8 T. (**b**) $C_p/T$ vs. $T$ curves of $GdMn_3Ni_2Mn_2O_{12}$ measured at $H$ = 0 and 9 T on cooling. The inset shows $C_p/T$ vs. $T$ curves at $H$ = 0, 3, 6, and 9 T.

Temperature dependence of specific heat and magnetic susceptibilities of $EuMn_3Ni_2Mn_2O_{12}$ is shown in Figure 6. Specific heat data clearly showed the presence of one magnetic transition at $T_N$ = 33 K; the specific heat anomaly was slightly dependent on magnetic fields. $\chi$ vs. $T$ curves showed a very small kink at $T_N$ = 33 K. On the other hand, differential $d\chi T/dT$ vs. $T$ curves allowed detecting the magnetic anomaly more clearly (the inset of Figure 6b). At high temperatures, inverse magnetic susceptibilities followed the Curie–Weiss law (Figure S5), and the obtained Curie–Weiss parameters (using the 7 T FCC curve in a temperature range of 250–350 K) were $\mu_{eff}$ = 11.216$\mu_B$ (the experimental effective magnetic moment) and $\theta$ = +0.1 K (the Curie–Weiss temperature). The $\mu_{eff}$ value was close to the expected calculated value of $\mu_{calc}$ = 11.382$\mu_B$ (taking 3.4$\mu_B$ for $Eu^{3+}$ [56]).

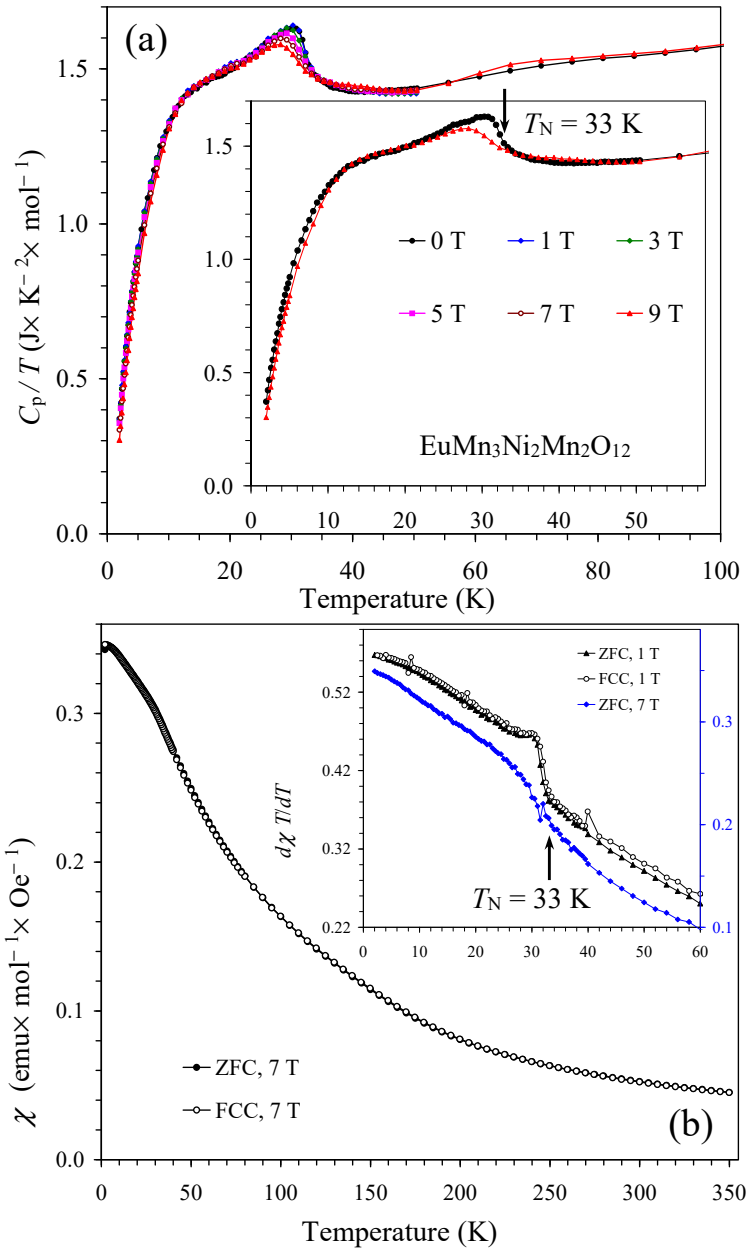


**Figure 6.** (**a**) $C_p/T$ vs. $T$ curves of $EuMn_3Ni_2Mn_2O_{12}$ measured at $H$ = 0, 1, 3, 5, 7, and 9 T on cooling. The inset shows $C_p/T$ vs. $T$ curves at $H$ = 0 and 9 T. The arrow shows a magnetic transition temperature. (**b**) ZFC (filled symbols) and FCC (empty symbols) dc magnetic susceptibility curves ($\chi = M/H$) of $EuMn_3Ni_2Mn_2O_{12}$ measured at $H$ = 7 T. The inset shows ZFC and FCC $d\chi T/dT$ vs. $T$ curves at $H$ = 1 T and 7 T.

Isothermal magnetization curves ($M$ vs. $H$) showed nearly linear behavior at $T$ = 5–200 K above about 1 T (Figure S5). The S-type shape was observed near the origin without any significant hysteresis originating from the impurity contribution with soft FM-like properties. Nearly the same S-type contribution was observed at $T$ = 5–100 K, that is, below and above $T_N$ = 33 K of $EuMn_3Ni_2Mn_2O_{12}$. On the other hand, the S-type shape near the origin disappeared at 200 K, that is, above the ferrimagnetic transition of the $(Eu_{1-x}Mn_x)MnO_3$ impurity. Therefore, the $\chi$ vs. $T$ and $M$ vs. $H$ curves give evidence that a purely AFM transition takes place in $EuMn_3Ni_2Mn_2O_{12}$ without any net FM-like moments.

Temperature dependence of the dielectric constant and loss tangent of $EuMn_3Ni_2Mn_2O_{12}$ (Figure 7) at different magnetic fields (0–8 T) showed no anomalies at $T_N$ = 33 K, suggesting the absence of any detectable (spin-induced) ferroelectric polarization.

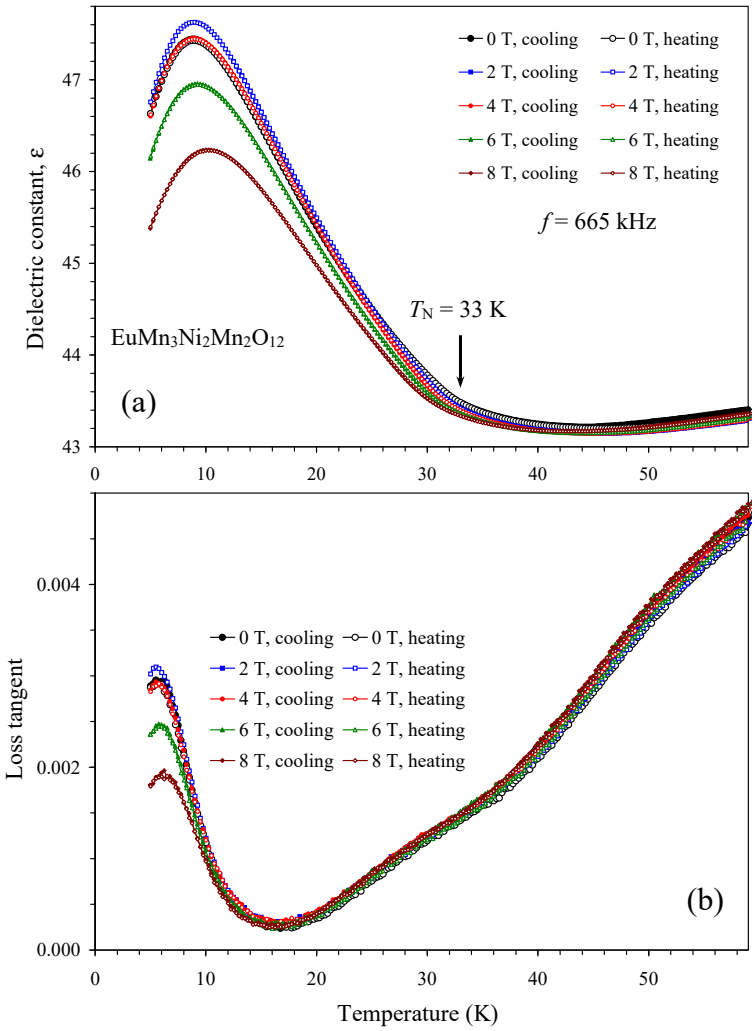


**Figure 7.** (**a**) Temperature dependence of dielectric constant of $EuMn_3Ni_2Mn_2O_{12}$ at one frequency of 665 kHz and different magnetic fields of 0, 2, 4, 6, and 8 T on cooling and heating. The arrow shows a magnetic transition temperature. (**b**) Temperature dependence of loss tangent of $EuMn_3Ni_2Mn_2O_{12}$ at one frequency of 665 kHz and different magnetic fields of 0, 2, 4, 6, and 8 T on cooling and heating.

### *2.4. R = Gd*

The dielectric constant of $GdMn_3Ni_2Mn_2O_{12}$ showed a small kink near $T_N$ = 22 K at $H$ = 0 T (Figures 8 and S6). The kink transforms to a weak peak already at $H$ = 1 T. The most pronounced peaks on dielectric constant and loss tangent were observed at $H$ = 5 T (Figures 8 and 9). Peaks on the dielectric constant disappear at $H$ = 8 and 9 T. Peaks on the dielectric constant clearly move to lower temperatures with increasing magnetic fields (peaks were observed at 23.2 K at 1 T, 23.0 K at 2 T, 22.5 K at 3 T, 21.5 K at 4 T, 20.5 K at 5 T, and 19.2 K at 6 T) in agreement with specific heat measurements (Figure 5b), confirming their common magnetic origin. Therefore, $GdMn_3Ni_2Mn_2O_{12}$ exhibits spin-induced ferroelectric polarization at about $H$ = 1–7 T.

### *2.5. R = Dy*

The temperature dependence of the dielectric constant and loss tangent of $DyMn_3Ni_2Mn_2O_{12}$ between $H$ = 0 T and $H$ = 8 T (Figure 10) was close to those of $EuMn_3Ni_2Mn_2O_{12}$ (Figure 6). No anomalies were observed at the magnetic transition temperatures of 36 K and 10 K [55].

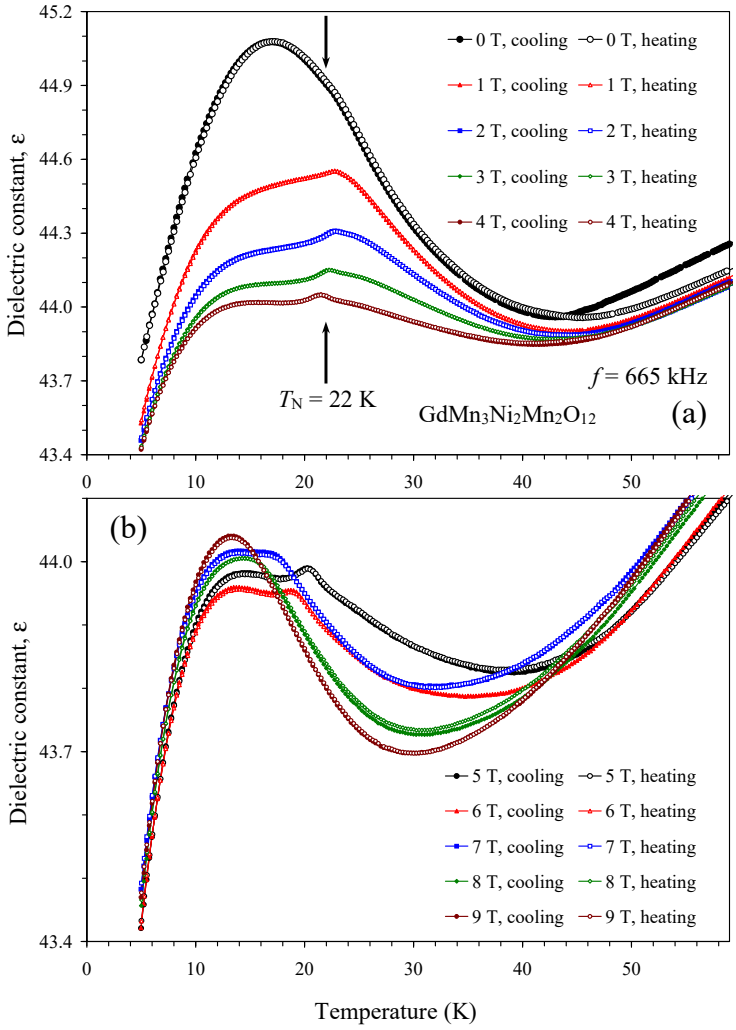


**Figure 8.** (**a**) Temperature dependence of dielectric constant of $GdMn_3Ni_2Mn_2O_{12}$ at one frequency of 665 kHz and different magnetic fields of 0, 1, 2, 3, and 4 T on cooling and heating. The arrow shows a magnetic transition temperature at $H$ = 0 T [55]. (**b**) Temperature dependence of dielectric constant of $GdMn_3Ni_2Mn_2O_{12}$ at one frequency of 665 kHz and different magnetic fields of 5, 6, 7, 8, and 9 T on cooling and heating.

### *2.6. R = Ho*

Temperature dependence of dielectric constant and loss tangent of $HoMn_3Ni_2Mn_2O_{12}$ between 0 T and 9 T is shown on Figures 11 and 12. Both dielectric constant and loss tangent showed small peaks near 36 K; this temperature matches with the magnetic transition temperature of $HoMn_3Ni_2Mn_2O_{12}$ [52], which was unambiguously determined with specific heat and magnetization measurements [52]. On the other hand, this temperature is also close to the magnetic and ferroelectric transition temperature of the $HoMn_2O_5$ impurity [57–60], which shows very strong and sharp anomalies on both dielectric constant and loss tangent [57–59]. The positions and intensities of the peaks remained nearly the same in all magnetic fields in $HoMn_3Ni_2Mn_2O_{12}$; and there was small hysteresis in the positions of the peaks on cooling and heating. Exactly the same behavior was observed in $HoMn_2O_5$ [57–59]. On the other hand, no hysteresis was observed on the temperature dependence of magnetic susceptibilities of $HoMn_3Ni_2Mn_2O_{12}$ [52] (we note that almost no anomalies were observed on magnetic susceptibilities of $HoMn_2O_5$ [59,60]). Therefore, we believe that there is a high probability that the observed anomalies on dielectric constant and loss tangent are caused by the $HoMn_2O_5$ impurity even though its amount was quite small (about 3 weight % [52]). Therefore, the intrinsic dielectric constant and loss tangent

of $HoMn_3Ni_2Mn_2O_{12}$ are very close to those of $DyMn_3Ni_2Mn_2O_{12}$; that is, there are no detectable anomalies at the magnetic transition temperature between 0 T and 9 T.

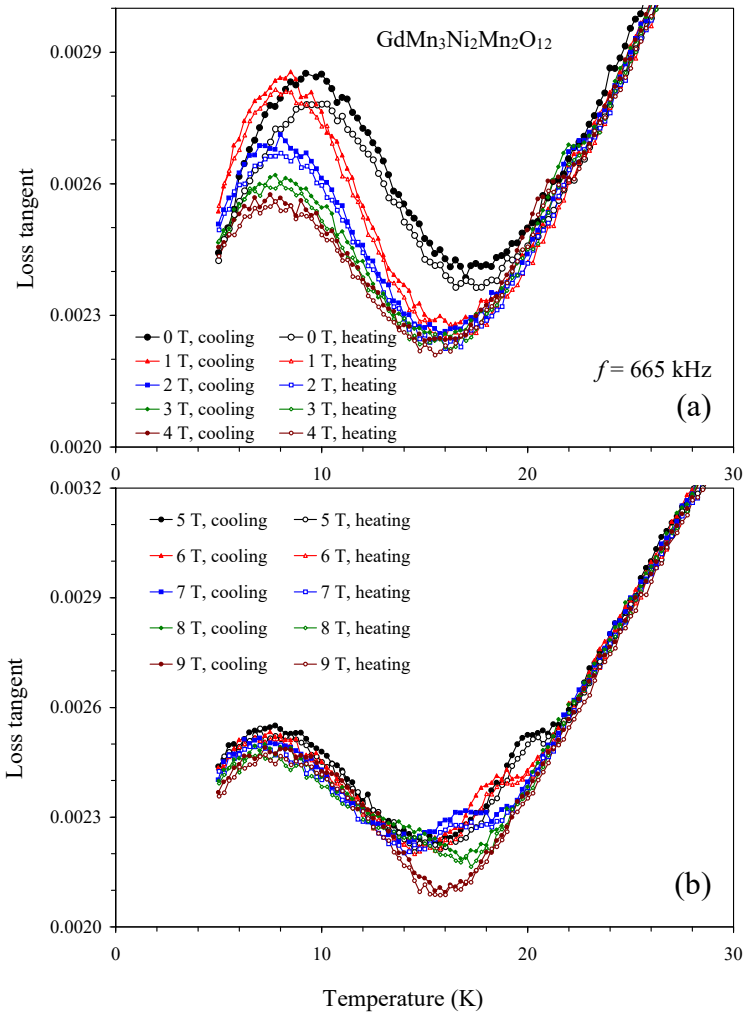


**Figure 9.** (**a**) Temperature dependence of loss tangent of $GdMn_3Ni_2Mn_2O_{12}$ at one frequency of 665 kHz and different magnetic fields of 0, 1, 2, 3, and 4 T on cooling and heating. (**b**) Temperature dependence of loss tangent of $GdMn_3Ni_2Mn_2O_{12}$ at one frequency of 665 kHz and different magnetic fields of 5, 6, 7, 8, and 9 T on cooling and heating.

### *2.7. $Lu_2NiMnO_6$*

For comparison, we report here the dielectric properties of one member of the $R_2NiMnO_6$ family with the smallest $R^{3+}$ cation of R = Lu. Specific heat measurements confirmed the presence of one FM transition at $T_C$ = 41 K (the inset of Figures 13b and S7). Dielectric properties of different members of the $R_2NiMnO_6$ family were reported in the literature [39,40], and no dielectric anomalies were usually observed. On the other hand, very detailed studies in the vicinity of $T_C$ demonstrated very weak kink-like anomalies at $T_C$ [25,36]; however, effects of magnetic fields have not been studied. Temperature dependence of the dielectric constant and loss tangent of our $Lu_2NiMnO_6$ sample, prepared by a high-pressure high-temperature method at 6 GPa, is shown in Figure 13. At $H$ = 0 T, we observed a very weak kink-like anomaly at $T_C$ similar to the previous reports [25,36]. The kink-like anomaly could originate from magnetostriction effects because $Lu_2NiMnO_6$ is a ferromagnet [61,62]. High magnetic fields smeared kink-like anomalies; for example, at $H$ = 7 T and 9 T, no visible dielectric anomalies were detected near $T_C$. Therefore, $Lu_2NiMnO_6$ does not develop ferroelectric polarization between 0 T and 9 T. The dielectric

constant decreases with decreasing temperature between 3 K and 300 K, as for ordinary insulators/dielectrics.

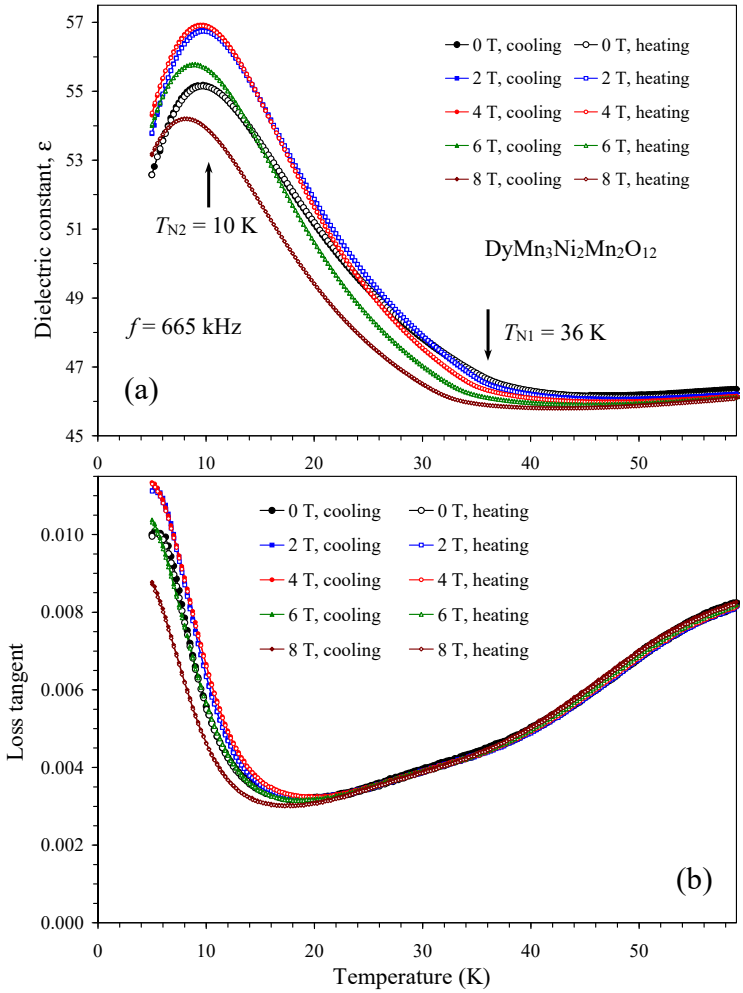


**Figure 10.** (**a**) Temperature dependence of dielectric constant of $DyMn_3Ni_2Mn_2O_{12}$ at one frequency of 665 kHz and different magnetic fields of 0, 2, 4, 6, and 8 T on cooling and heating. The arrows show the magnetic transition temperatures at $H$ = 0 T [55]. (**b**) Temperature dependence of loss tangent of $DyMn_3Ni_2Mn_2O_{12}$ at one frequency of 665 kHz and different magnetic fields of 0, 2, 4, 6, and 8 T on cooling and heating.

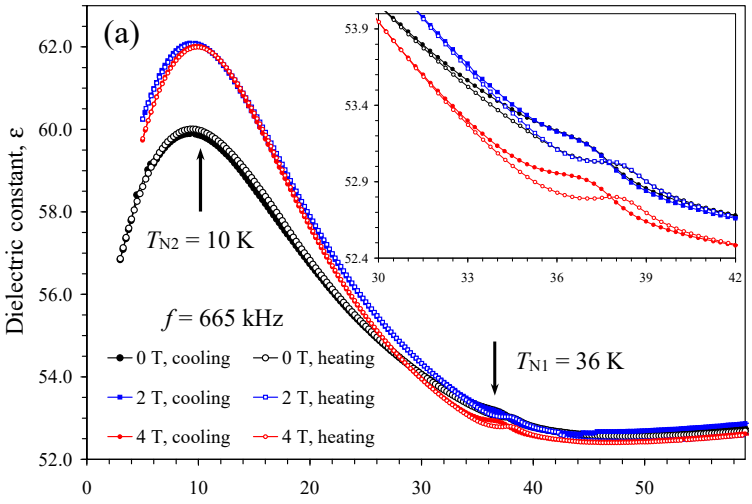


**Figure 11.** *Cont.*

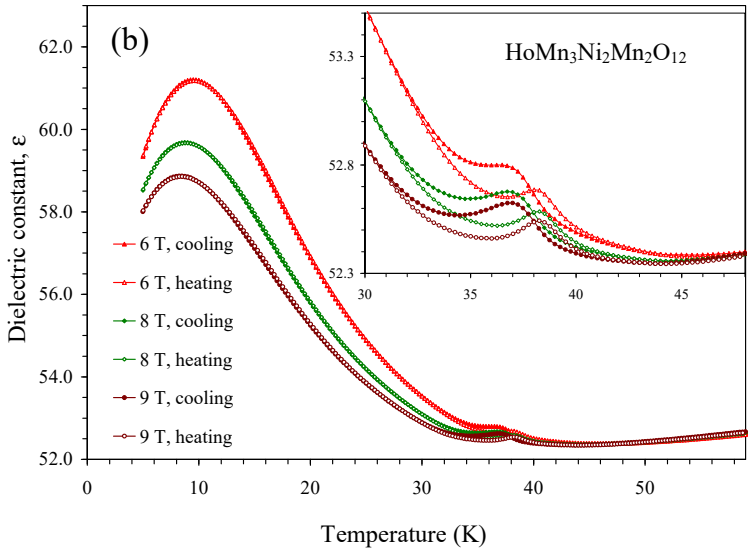


**Figure 11.** (**a**) Temperature dependence of dielectric constant of $HoMn_3Ni_2Mn_2O_{12}$ at one frequency of 665 kHz and different magnetic fields of 0, 2, and 4 T on cooling and heating. The arrows show the magnetic transition temperatures [52]. (**b**) Temperature dependence of the dielectric constant of $HoMn_3Ni_2Mn_2O_{12}$ at one frequency of 665 kHz and different magnetic fields of 6, 8, and 9 T on cooling and heating. The insets show magnified parts.

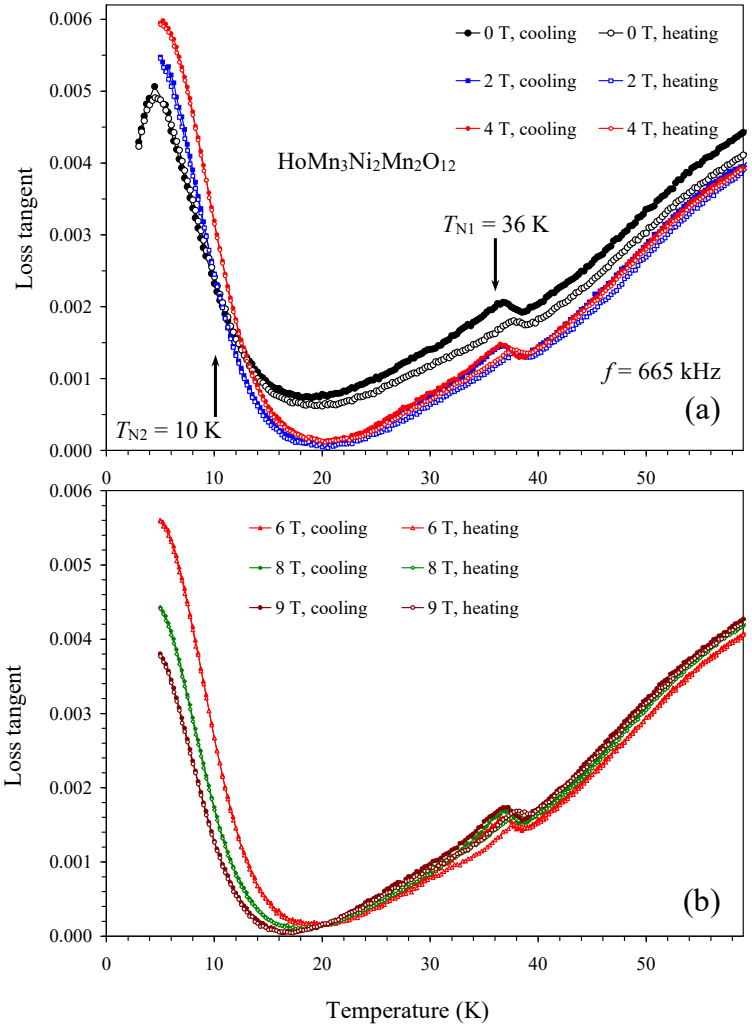


**Figure 12.** (**a**) Temperature dependence of loss tangent of $HoMn_3Ni_2Mn_2O_{12}$ at one frequency of 665 kHz and different magnetic fields of 0, 2, and 4 T on cooling and heating. The arrows show the

magnetic transition temperatures [52]. (**b**) Temperature dependence of loss tangent of $HoMn_3Ni_2Mn_2O_{12}$ at one frequency of 665 kHz and different magnetic fields of 6, 8, and 9 T on cooling and heating.

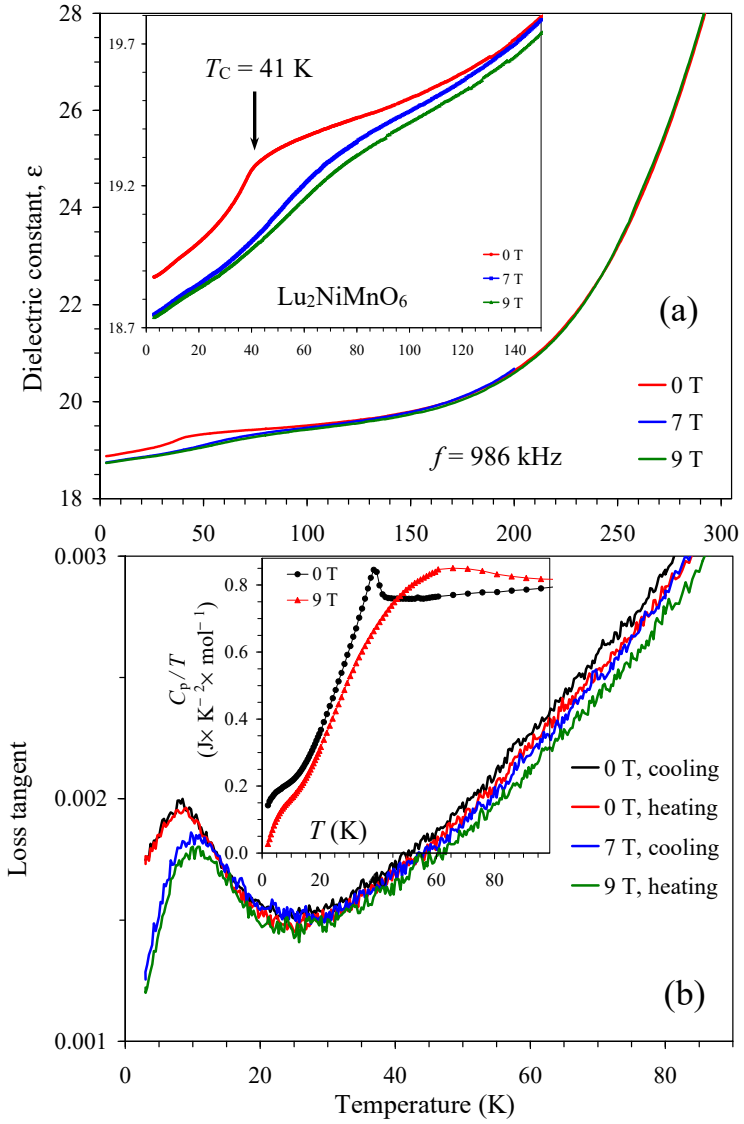


**Figure 13.** Temperature dependence of (**a**) dielectric constant and (**b**) loss tangent at one frequency of 986 kHz in $Lu_2NiMnO_6$ at $H$ = 0, 7, and 9 T in different temperature ranges. The inset in the panel (**a**) shows details below 150 K, where the arrow shows a ferromagnetic transition temperature. The inset in the panel (**b**) shows $C_p/T$ vs. $T$ curves of $Lu_2NiMnO_6$ at $H$ = 0 and 9 T.

## 3. Materials and Methods

$RMn_3Ni_2Mn_2O_{12}$ samples with R = Bi, Ce, Nd, Sm, Eu, Gd, Dy, and Ho were prepared from stoichiometric mixtures of $Bi_2O_3$ (Rare Metallic Co., Tokyo, Japan, 99.9999%), $CeO_2$ (Rare Metallic Co., Tokyo, Japan, 99.99%), $R_2O_3$ (Rare Metallic Co., Tokyo, Japan, 99.9%), $Mn_2O_3$ (Rare Metallic Co., Tokyo, Japan, 99.99%), $MnO_2$ (Alfa Aesar, Ward Hill, MA, USA, 99.99%), and NiO (Rare Metallic Co., Tokyo, Japan, 99.9%). Single-phase $Mn_2O_3$ was prepared from a commercial $MnO_2$ chemical (Rare Metallic Co., Tokyo, Japan, 99.99%) by annealing in air at 923 K for 24 h. The synthesis was performed at about 6 GPa and at about 1500 K for 2 h in sealed Au capsules using a belt-type HP instrument. After annealing at 1500 K, the samples were cooled down to room temperature by turning off the heating current, and the pressure was slowly released.

The $Lu_2NiMnO_6$ sample was prepared from stoichiometric mixtures of $Lu_2O_3$ (Rare Metallic Co., Tokyo, Japan, 99.9%), $MnO_2$ (Alfa Aesar, Ward Hill, MA, USA, 99.99%), and NiO (Rare Metallic Co., Tokyo, Japan, 99.9%) by the high-pressure high-temperature method at about 6 GPa and at about 1700 K for 2 h in a sealed Pt capsule. We note that the oxygen content and purity of $MnO_2$ (Alfa Aesar, Ward Hill, MA, USA, 99.99%) were confirmed before its use by the thermogravimetric analysis and X-ray powder diffraction. The refined lattice parameters of $Lu_2NiMnO_6$ (space group $P2_1/n$ with $a$ = 5.1490(1) Å, $b$ = 5.5123(1) Å, $c$ = 7.4073(1) Å, and $\beta$ = 90.441(1)°) were close to the reported values [35].

X-ray powder diffraction data of $EuMn_3Ni_2Mn_2O_{12}$ were collected at room temperature on a MiniFlex600-C diffractometer (Rigaku, Tokyo, Japan) using CuK$\alpha$ radiation (a 2$\theta$ range of 10–120°, a step width of 0.02°, and a scan speed of 3°/min; and a 2$\theta$ range of 38–44°, a step width of 0.02°, and a scan speed of 0.1 °/min) (Figure S8). The Rietveld analysis of all X-ray powder diffraction data was performed using the *RIETAN-2000* program [63]. The crystallographic characterization of other samples was reported in [52,55].

Magnetic measurements of $EuMn_3Ni_2Mn_2O_{12}$ were performed on SQUID magnetometers (Quantum Design MPMS3, San Diego, CA, USA) between 2 K and 350 K (and between 330 K and 750 K) in applied fields of 0.01 T, 1 T, and 7 T under both zero-field-cooled (ZFC) and field-cooled on cooling (FCC) conditions. Magnetic-field dependence was measured at different temperatures between −7 T and +7 T. Specific heat, $C_p$, of $RMn_3Ni_2Mn_2O_{12}$ was measured on cooling from 100 K to 2 K at different magnetic fields from 0 T to 9 T by a pulse relaxation method using a commercial calorimeter (Quantum Design PPMS, San Diego, CA, USA).

Dielectric properties were measured using an Alpha-A High Performance Frequency Analyzer (NOVOCONTROL Technologies, Montabaur, Germany) on cooling and heating in a temperature range between 3–5 K and 70–300 K and a frequency range from 100 Hz to 665 kHz (or 986 kHz) at different magnetic fields from 0 T to 9 T. Pieces of pellets were used in all magnetic, specific heat, and dielectric measurements.

## 4. Conclusions

Dielectric properties of the A-site-ordered quadruple perovskites, $RMn_3Ni_2Mn_2O_{12}$ with R = Bi, Ce, Nd, Sm, Eu, Gd, Dy, and Ho, were investigated at different magnetic fields between 0 T and 9 T. A principal difference in the temperature dependence of the dielectric constant was observed for R = Bi, Ce, and Nd and for R = Sm, Eu, Gd, Dy, and Ho. The dielectric constant of the former group decreases with decreasing temperature down to the lowest temperature. The dielectric constant of the latter group starts increasing with decreasing temperature when approaching magnetic transition temperatures, suggesting different magnetic ground states. Peak-like anomalies were found on dielectric constant and loss tangent in intermediate magnetic-field ranges for the R = Sm and Gd samples, suggesting the existence of "hidden" [64] magnetic-field-induced multiferroic states. Physical properties of a new compound, $EuMn_3Ni_2Mn_2O_{12}$, were also investigated with specific heat and magnetization measurements. Dielectric properties of $Lu_2NiMnO_6$ at different magnetic fields are reported for comparison.

**Supplementary Materials:** The following supporting information can be downloaded at: https://www.mdpi.com/article/10.3390/inorganics13100315/s1. Figure S1: Temperature dependence of (a) dielectric constant and (b) loss tangent of $NdMn_3Ni_2Mn_2O_{12}$ at different frequencies from 100 Hz to 665 kHz. Measurements were performed on cooling at $H$ = 0 T; Figure S2: Temperature dependence of dielectric constant of $SmMn_3Ni_2Mn_2O_{12}$ at different frequencies from 100 Hz to 665 kHz. Measurements were performed on cooling at (a) $H$ = 0 T and at (b) $H$ = 8 T; Figure S3: Temperature dependence of loss tangent of $SmMn_3Ni_2Mn_2O_{12}$ at different frequencies from 100 Hz to 665 kHz. Measurements were performed on cooling at (a) $H$ = 0 T and at (b) $H$ = 8 T; Figure S4:

Temperature dependence of dielectric constant of $SmMn_3Ni_2Mn_2O_{12}$ at one frequency of 665 kHz and different magnetic fields of (a) 0, 1, 2, 3, and 4 T and (b) 5, 6, 7, 8, and 9 T on cooling and heating. Different measurements (from Figure 4 in the main text and from Figures S2 and S3) are reported. Temperature dependence of loss tangent of $SmMn_3Ni_2Mn_2O_{12}$ at one frequency of 665 kHz and different magnetic fields of (c) 0, 1, 2, 3, and 4 T and (d) only at 0 and 1 T (to emphasize the absence of anomalies) on cooling and heating. (e) Temperature dependence of loss tangent of $SmMn_3Ni_2Mn_2O_{12}$ at one frequency of 665 kHz and different magnetic fields of 5, 6, 7, 8, and 9 T; Figure S5: (a) $M$ vs. $H$ curves of $EuMn_3Ni_2Mn_2O_{12}$ at $T$ = 5 K, 20 K, 40 K, 60 K, 100 K, and 200 K. The inset shows a magnified part of the $M$ vs. $H$ curves at $T$ = 5 K and 20 K. (b) $M$ vs. $H$ curves of $EuMn_3Ni_2Mn_2O_{12}$ at $T$ = 5 K and 20 K, below its $T_N$ = 33 K. The S-type shape of the $M$ vs. $H$ curves near the origin comes from a contribution from the ferrimagnetic impurity $(Eu_{1-x}Mn_x)MnO_3$ (space group *Pnma*); otherwise, the $M$ vs. $H$ curves were linear without hysteresis. (c) Inverse magnetic susceptibilities of $EuMn_3Ni_2Mn_2O_{12}$ measured at magnetic fields of $H$ = 100 Oe, 10 kOe, and 70 kOe in the low-temperature (LT) region of 2–350 K and in the high-temperature (HT) region of 330–750 K. Red lines show the Curie–Weiss fittings of the LT and HT data at $H$ = 70 kOe; fitting parameters are shown on this figure. The anomaly near 140 K on the LT region originates from the ferrimagnetic impurity $(Eu_{1-x}Mn_x)MnO_3$. A very weak anomaly near 400 K, seen on the HT data at $H$ = 100 Oe, could originate from traces of $NiMnO_3$ impurity observed in some other samples of $RMn_3Ni_2Mn_2O_{12}$ with R = Bi, Ce, and Ho. Magnetic measurements showed that the amount of a possible $NiMnO_3$ impurity was very small, well below the detection limit of laboratory X-ray diffraction; Figure S6: Temperature dependence of dielectric constant of $GdMn_3Ni_2Mn_2O_{12}$ at different frequencies from 100 Hz to 665 kHz. Measurements were performed on heating at (a) $H$ = 0 T and at (b) $H$ = 5 T; Figure S7: $C_p/T$ vs. $T$ curves of $Lu_2NiMnO_6$ at different magnetic fields of $H$ = 0, 0.2, 1, 2, 3, 5, and 9 T. Measurements were performed on cooling; Figure S8: (a) Experimental (black crosses), calculated (red line), and difference (blue line at the bottom) room-temperature laboratory X-ray powder diffraction patterns of $EuMn_3Ni_2Mn_2O_{12}$ (space group $Pn-3$) in a $2\theta$ range of 16° and 120°. The tick marks show possible Bragg reflection positions for the main phase (brown), $(Eu_{1-x}Mn_x)MnO_3$ impurity (blue), and NiO impurity (green) (from top to bottom). (b) A magnified part of the experimental and calculated patterns in a $2\theta$ range of 38° and 44°, emphasizing the presence of the (311) reflection from the (partial) B-site ordering. The data between 38° and 44° were measured with a speed of 0.1°/min and scaled to match with other data (panel (a)) measured with a speed of 3°/min; because of scaling, the background on panel (b) was not fitted well.

**Author Contributions:** Conceptualization, A.A.B.; methodology, A.A.B.; validation, A.A.B.; formal analysis, A.A.B.; investigation, A.A.B., R.L., and K.Y.; resources, K.Y.; data curation, A.A.B.; writing—original draft preparation, A.A.B.; writing—review and editing, A.A.B.; supervision, A.A.B. and K.Y.; project administration, A.A.B.; funding acquisition, K.Y. All authors have read and agreed to the published version of the manuscript.

**Funding:** This work was partially supported by a Grant-in-Aid for Scientific Research (No. JP25K01657) from the Japan Society for the Promotion of Science.

**Institutional Review Board Statement:** Not applicable.

**Informed Consent Statement:** Not applicable.

**Data Availability Statement:** The original data presented in this study are openly available on Zenodo at https://doi.org/10.5281/zenodo.17131358.

**Acknowledgments:** MANA was supported by the World Premier International Research Center Initiative (WPI), MEXT, Japan.

**Conflicts of Interest:** The author declares no conflicts of interest.

## References

1. Schmid, H. Multi-ferroic magnetoelectrics. *Ferroelectrics* **1994**, *162*, 317–338. [CrossRef]
2. Eerenstein, W.; Mathur, N.; Scott, J.F. Multiferroic and magnetoelectric materials. *Nature* **2006**, *442*, 759–765. [CrossRef]

3. Khomskii, D.I. Multiferroics: Different ways to combine magnetism and ferroelectricity. *J. Magn. Magn. Mater.* **2006**, *306*, 1–8. [CrossRef]
4. Cheong, S.-W.; Mostovoy, M. Multiferroics: A magnetic twist for ferroelectricity. *Nat. Mater.* **2007**, *6*, 13–20. [CrossRef]
5. Khomskii, D. Classifying multiferroics: Mechanisms and effects. *Physics* **2009**, *2*, 20. [CrossRef]
6. Tokura, Y.; Seki, S.; Nagaosa, N. Multiferroics of spin origin. *Rep. Prog. Phys.* **2014**, *77*, 076501. [CrossRef]
7. Fiebig, M.; Lottermoser, T.; Meier, D.; Trassin, M. The evolution of multiferroics. *Nat. Rev. Mater.* **2016**, *1*, 16046. [CrossRef]
8. Heron, J.T.; Trassin, M.; Ashraf, K.; Gajek, M.; He, Q.; Yang, S.Y.; Nikonov, D.E.; Chu, Y.; Salahuddin, H.S.; Ramesh, R. Electric-field-induced magnetization reversal in a ferromagnet-multiferroic heterostructure. *Phys. Rev. Lett.* **2011**, *107*, 217202. [CrossRef]
9. Ueland, B.G.; Lynn, J.W.; Laver, M.; Choi, Y.J.; Cheong, S.-W. Origin of electric-field-induced magnetization in multiferroic $HoMnO_3$. *Phys. Rev. Lett.* **2010**, *104*, 147204. [CrossRef]
10. Kimura, T.; Goto, T.; Shintani, H.; Ishizaka, K.; Arima, T.; Tokura, Y. Magnetic control of ferroelectric polarization. *Nature* **2003**, *426*, 55–58. [CrossRef] [PubMed]
11. Kenzelmann, M.; Harris, A.B.; Jonas, S.; Broholm, C.; Schefer, J.; Kim, S.B.; Zhang, C.L.; Cheong, S.-W.; Vajk, O.P.; Lynn, J.W. Magnetic inversion symmetry breaking and ferroelectricity in $TbMnO_3$. *Phys. Rev. Lett.* **2005**, *95*, 087206. [CrossRef]
12. Pomjakushin, V.Y.; Kenzelmann, M.; Dönni, A.; Harris, A.B.; Nakajima, T.; Mitsuda, S.; Tachibana, M.; Keller, L.; Mesot, J.; Kitazawa, H.; et al. Evidence for large electric polarization from collinear magnetism in $TmMnO_3$. *New J. Phys.* **2009**, *11*, 043019. [CrossRef]
13. Mukherjee, S.; Dönni, A.; Nakajima, T.; Mitsuda, S.; Tachibana, M.; Kitazawa, H.; Pomjakushin, V.; Keller, L.; Niedermayer, C.; Scaramucci, A.; et al. E-type noncollinear magnetic ordering in multiferroic o-$LuMnO_3$. *Phys. Rev. B* **2017**, *95*, 104412. [CrossRef]
14. Tokunaga, Y.; Iguchi, S.; Arima, T.; Tokura, Y. Magnetic-field-induced ferroelectric state in $DyFeO_3$. *Phys. Rev. Lett.* **2008**, *101*, 097205. [CrossRef] [PubMed]
15. Tokunaga, Y.; Taguchi, Y.; Arima, T.H.; Tokura, Y. Electric-field-induced generation and reversal of ferromagnetic moment in ferrites. *Nat. Phys.* **2012**, *8*, 838–844. [CrossRef]
16. Bousquet, E.; Cano, A. Non-collinear magnetism in multiferroic perovskites. *J. Phys. Condens. Matter* **2016**, *28*, 123001. [CrossRef] [PubMed]
17. Lee, J.-H.; Jeong, Y.K.; Park, J.H.; Oak, M.-A.; Jang, H.M.; Son, J.Y.; Scott, J.F. Spin-canting-induced improper ferroelectricity and spontaneous magnetization reversal in $SmFeO_3$. *Phys. Rev. Lett.* **2011**, *107*, 117201. [CrossRef]
18. Johnson, R.D.; Terada, N.; Radaelli, P.G. Comment on "Spin-canting-induced improper ferroelectricity and spontaneous magnetization reversal in $SmFeO_3$". *Phys. Rev. Lett.* **2012**, *108*, 219701. [CrossRef] [PubMed]
19. Kuo, C.-Y.; Drees, Y.; Fernández-Díaz, M.T.; Zhao, L.; Vasylechko, L.; Sheptyakov, D.; Bell, A.M.T.; Pi, T.W.; Lin, H.-J.; Wu, M.-K.; et al. k = 0 magnetic structure and absence of ferroelectricity in $SmFeO_3$. *Phys. Rev. Lett.* **2014**, *113*, 217203. [CrossRef]
20. Rajeswaran, B.; Sanyal, D.; Chakrabarti, M.; Sundarayya, Y.; Sundaresan, A.; Rao, C.N.R. Interplay of 4f-3d magnetism and ferroelectricity in $DyFeO_3$. *EPL* **2013**, *101*, 17001. [CrossRef]
21. Saha, R.; Sundaresan, A.; Rao, C.N.R. Novel features of multiferroic and magnetoelectric ferrites and chromites exhibiting magnetically driven ferroelectricity. *Mater. Horiz.* **2014**, *1*, 20–31. [CrossRef]
22. Oliveira, G.N.P.; Teixeira, R.C.; Moreira, R.P.; Correia, J.G.; Araújo, J.P.; Lopes, A.M.L. Local inhomogeneous state in multiferroic $SmCrO_3$. *Sci. Rep.* **2020**, *10*, 4686. [CrossRef]
23. Zvezdin, A.K.; Gareeva, Z.V.; Chen, X.M. Multiferroic order parameters in rhombic antiferromagnets $RCrO_3$. *J. Phys. Condens. Matter* **2021**, *33*, 385801. [CrossRef]
24. Prado-Gonjal, J.; Schmidt, R.; Romero, J.-J.; Ávila, D.; Amador, U.; Morán, E. Microwave-assisted synthesis, microstructure, and physical properties of rare-earth chromites. *Inorg. Chem.* **2013**, *52*, 313–320. [CrossRef]
25. Zhang, C.; Zhang, T.; Ge, L.; Wang, S.; Yuan, H.; Feng, S. Hydrothermal synthesis and multiferroic properties of $Y_2NiMnO_6$. *RSC Adv.* **2014**, *4*, 50969–50974. [CrossRef]
26. Su, J.; Yang, Z.; Lu, X.; Zhang, J.; Gu, L.; Lu, C.; Li, Q.; Liu, J.; Zhu, J. Magnetism-driven ferroelectricity in double perovskite $Y_2NiMnO_6$. *ACS Appl. Mater. Interfaces* **2015**, *7*, 13260–13265. [CrossRef]
27. Nhalil, H.; Nair, H.S.; Kumar, C.M.N.; Strydom, A.M.; Elizabeth, S. Ferromagnetism and the effect of free charge carriers on electric polarization in the double perovskite $Y_2NiMnO_6$. *Phys. Rev. B* **2015**, *92*, 214426. [CrossRef]
28. Sánchez-Benítez, J.; Martínez-Lope, M.J.; Alonso, J.A.; García-Muñoz, J.L. Magnetic and structural features of the $NdNi_{1-x}Mn_xO_3$ perovskite series investigated by neutron diffraction. *J. Phys. Condens. Matter* **2011**, *23*, 226001. [CrossRef] [PubMed]
29. Retuerto, M.; Muñoz, Á.; Martínez-Lope, M.J.; Alonso, J.A.; Mompeán, F.J.; Fernández-Díaz, M.T.; Sánchez-Benítez, J. Magnetic interactions in the double perovskites $R_2NiMnO_6$ (R = Tb, Ho, Er, Tm) investigated by neutron diffraction. *Inorg. Chem.* **2015**, *54*, 10890–10900. [CrossRef] [PubMed]

30. Booth, R.J.; Fillman, R.; Whitaker, H.; Nag, A.; Tiwari, R.M.; Ramanujachary, K.V.; Gopalakrishnan, J.; Lofland, S.E. An investigation of structural, magnetic and dielectric properties of $R_2NiMnO_6$ (R = rare earth, Y). *Mater. Res. Bull.* **2009**, *44*, 1559–1564. [CrossRef]
31. Nasir, M.; Kumar, S.; Patra, N.; Bhattacharya, D.; Jha, S.N.; Basaula, D.R.; Bhatt, S.; Khan, M.; Liu, S.-W.; Biring, S.; et al. Role of antisite disorder, rare-earth size, and superexchange angle on band gap, Curie temperature, and magnetization of $R_2NiMnO_6$ double perovskites. *ACS Appl. Electron. Mater.* **2019**, *1*, 141–153. [CrossRef]
32. Asai, K.; Fujiyoshi, K.; Nishimori, N.; Satoh, Y.; Kobayashi, Y.; Mizoguchi, M. Magnetic properties of $REMe_{0.5}Mn_{0.5}O_3$ (RE = rare earth element, Me = Ni, Co). *J. Phys. Soc. Jpn.* **1998**, *67*, 4218–4228. [CrossRef]
33. Sobolev, A.V.; Glazkova, I.S.; Akulenko, A.A.; Sergueev, I.; Chumakov, A.I.; Yi, W.; Belik, A.A.; Presniakov, I.A. $^{61}$Ni nuclear forward scattering study of magnetic hyperfine interactions in double perovskites $A_2NiMnO_6$ (A = Sc, In, Tl). *J. Phys. Chem.* **2019**, *123*, 23628–23634. [CrossRef]
34. Ding, L.; Khalyavin, D.D.; Manuel, P.; Blake, J.; Orlandi, F.; Yi, W.; Belik, A.A. Colossal magnetoresistance in the insulating ferromagnetic double perovskites $Tl_2NiMnO_6$: A neutron diffraction study. *Acta Mater.* **2019**, *173*, 20–26. [CrossRef]
35. Terada, N.; Colin, C.V.; Qureshi, N.; Hansen, T.; Matsubayashi, K.; Uwatoko, Y.; Belik, A.A. Pressure-induced incommensurate antiferromagnetic order in a ferromagnetic B-site ordered double-perovskite $Lu_2NiMnO_6$. *Phys. Rev. B* **2020**, *102*, 094412. [CrossRef]
36. Zhang, C.; Zhu, W.; Yuan, L.; Yuan, H. B-site ordering, magnetic and dielectric properties of hydrothermally synthesized $Lu_2NiMnO_6$. *J. Alloys Compd.* **2018**, *744*, 395–403. [CrossRef]
37. Chanda, S.; Saha, S.; Dutta, A.; Murthy, J.K.; Venimadhav, A.; Shannigrahi, S.; Sinha, T.P. Magnetic ordering and conduction mechanism of different electroactive regions in $Lu_2NiMnO_6$. *J. Appl. Phys.* **2016**, *120*, 134102. [CrossRef]
38. Zhang, L.; Shi, T.L.; Cao, J.J.; Yan, S.M.; Fang, Y.; Han, Z.D.; Qian, B.; Jiang, X.F.; Wang, D.H. Critical behavior and magnetocaloric effect in the multiferroic double perovskite $Lu_2NiMnO_6$. *J. Alloys Compd.* **2018**, *763*, 613–621. [CrossRef]
39. Katari, V.; Babu, P.D.; Mishra, S.K.; Mittal, R.; Bevara, S.; Achary, S.N.; Deshpande, S.K.; Tyagi, A.K. Effect of preparation conditions on magnetic and dielectric properties of $Y_2MMnO_6$ (M = Co, Ni). *J. Am. Ceram. Soc.* **2016**, *99*, 499–506. [CrossRef]
40. Kakarla, D.C.; Jyothinagaram, K.M.; Das, A.K.; Adyam, V. Dielectric and magnetodielectric properties of $R_2NiMnO_6$ (R = Nd, Eu, Gd, Dy, and Y). *J. Am. Ceram. Soc.* **2014**, *97*, 2858–2866. [CrossRef]
41. Zhang, C.Y.; Wang, Z.Z.; Yuan, L.; Ti, R.X.; Wu, H.R.; Yuan, H.M. Double perovskites $R_2NiMnO_6$ with small $R^{3+}$ cations: Magnetic interactions tuned by $R^{3+}$ ionic radius and the role of orbital ordering. *J. Alloys Compd.* **2025**, *1039*, 182997. [CrossRef]
42. Shannon, R.D. Revised effective ionic radii and systematic studies of interatomic distances in halides and chalcogenides. *Acta Crystall. A* **1976**, *32*, 751–767. [CrossRef]
43. Yi, W.; Princep, A.J.; Guo, Y.F.; Johnson, R.D.; Khalyavin, D.D.; Manuel, P.; Senyshyn, A.; Presniakov, I.A.; Sobolev, A.V.; Matsushita, Y.; et al. $Sc_2NiMnO_6$: A double-perovskite with a magnetodielectric response driven by multiple magnetic orders. *Inorg. Chem.* **2015**, *54*, 8012–8021. [CrossRef] [PubMed]
44. Yi, W.; Liang, Q.F.; Matsushita, Y.; Tanaka, M.; Belik, A.A. High-pressure synthesis, crystal structure, and properties of $In_2NiMnO_6$ with antiferromagnetic order and field-induced phase transition. *Inorg. Chem.* **2013**, *52*, 14108–14115. [CrossRef] [PubMed]
45. Terada, N.; Khalyavin, D.D.; Manuel, P.; Yi, W.; Suzuki, H.S.; Tsujii, N.; Imanaka, Y.; Belik, A.A. Ferroelectricity induced by ferriaxial crystal rotation and spin helicity in a B-site-ordered double-perovskite multiferroic $In_2NiMnO_6$. *Phys. Rev. B* **2015**, *91*, 104413. [CrossRef]
46. Vasil'ev, A.N.; Volkova, O.S. New functional materials $AC_3B_4O_{12}$ (Review). *Low Temp. Phys.* **2007**, *33*, 895–914. [CrossRef]
47. Long, Y. A-site ordered quadruple perovskite oxides $AA'_3B_4O_{12}$. *Chin. Phys. B* **2016**, *25*, 078108. [CrossRef]
48. Yamada, I. Novel catalytic properties of quadruple perovskites. *Sci. Technol. Adv. Mater.* **2017**, *18*, 541–548. [CrossRef]
49. Belik, A.A.; Johnson, R.D.; Khalyavin, D.D. The rich physics of A-site-ordered quadruple perovskite manganites $AMn_7O_{12}$. *Dalton Trans.* **2021**, *50*, 15458–15472. [CrossRef]
50. Solana-Madruga, E.; Arevalo-Lopez, A.M. High-pressure A-site manganites: Structures and magnetic properties. *J. Solid State Chem.* **2022**, *315*, 123470. [CrossRef]
51. Ding, J.; Zhu, X.H. Research progress on quadruple perovskite oxides. *J. Mater. Chem. C* **2024**, *12*, 9510–9561. [CrossRef]
52. Belik, A.A. A site-ordered quadruple perovskites, $RMn_3Ni_2Mn_2O_{12}$ with R = Bi, Ce, and Ho, with different degrees of B site ordering. *Molecules* **2025**, *30*, 1749. [CrossRef]
53. Yin, Y.Y.; Liu, M.; Dai, J.H.; Wang, X.; Zhou, L.; Cao, H.; Cruz, C.D.; Chen, C.T.; Xu, Y.; Shen, X.; et al. $LaMn_3Ni_2Mn_2O_{12}$: An A-and B-site ordered quadruple perovskite with A-site tuning orthogonal spin ordering. *Chem. Mater.* **2016**, *28*, 8988–8996. [CrossRef]
54. Liu, M.; Hu, C.-E.; Cheng, C.; Chen, X.R. A–B-intersite-dependent magnetic order and electronic structure of $LaMn_3Ni_2Mn_2O_{12}$: A first-principles study. *J. Phys. Chem. C* **2018**, *122*, 1946–1954. [CrossRef]
55. Belik, A.A.; Liu, R.; Tanaka, M.; Yamaura, K. B-site-ordered and disordered structures in A-site-ordered quadruple perovskites $RMn_3Ni_2Mn_2O_{12}$ with R = Nd, Sm, Gd, and Dy. *Molecules* **2024**, *29*, 5488. [CrossRef]

56. Kittel, C.; McEuen, P. *Introduction to Solid State Physics*; John Wiley & Sons, Inc.: New York, NY, USA, 2005.
57. Higashiyama, D.; Miyasaka, S.; Tokura, Y. Magnetic-field-induced polarization and depolarization in $HoMn_2O_5$ and $ErMn_2O_5$. *Phys. Rev. B* **2005**, *72*, 064421. [CrossRef]
58. Mihailova, B.; Gospodinov, M.M.; Güttler, B.; Yen, F.; Litvinchuk, A.P.; Iliev, M.N. Temperature-dependent Raman spectra of $HoMn_2O_5$ and $TbMn_2O_5$. *Phys. Rev. B* **2005**, *71*, 172301. [CrossRef]
59. Radulov, I.; Nizhankovskii, V.I.; Lovchinov, V.; Dimitrov, D.; Apostolov, A. Colossal magnetostriction effect in $HoMn_2O_5$. *Eur. Phys. J. B* **2006**, *52*, 361–364. [CrossRef]
60. Tzankov, D.; Skumryev, V.; Aroyo, M.; Puzniak, R.; Kuz'min, M.D.; Mikhov, M. Magnetic anisotropy of multiferroic $HoMn_2O_5$ single crystal. *Solid State Commun.* **2008**, *147*, 212–216. [CrossRef]
61. Boldrin, M.; Bagri, A.; Barlettani, D.; Teather, E.; Squillante, L.; de Souza, M.; Pontes, R.B.; Silva, A.G.; Mori, T.J.A.; Perry, R.; et al. Magnetostriction as the origin of the magnetodielectric effect in $La_2CoMnO_6$. *Phys. Rev. Mater.* **2025**, *9*, 094403. [CrossRef]
62. Manikandan, M.; Ghosh, A.; Mahendiran, R. Giant magnetostriction in $La_2CoMnO_6$ synthesized by microwave irradiation. *Appl. Phys. Lett.* **2023**, *123*, 022403. [CrossRef]
63. Izumi, F.; Ikeda, T. A Rietveld-analysis program RIETAN-98 and its applications to zeolites. *Mater. Sci. Forum* **2000**, *321–324*, 198–205. [CrossRef]
64. Kumar, R.; Sundaresan, A. Unveiling a hidden multiferroic state under magnetic fields in $BaHoFeO_4$. *Phys. Rev. B* **2023**, *107*, 184420. [CrossRef]